MOLECULAR BIOLOGY

Bursty gene expression and mRNA decay pathways orchestrate B cell activation

Yi Zhou and Cornelis Murre*

It is well established that the helix-loop-helix proteins, E2A and E2-2, promote B cell activation. Here, we examined how during the course of B cell activation *E2A* and *E2-2* gene expression is regulated. We found that *E2A* and *E2-2* mRNA abundance concomitantly increased in activated B cells. The increase in *E2A* and *E2-2* mRNA abundance correlated with increased cell growth. Elevated *E2A* and *E2-2* mRNA abundance was instructed by increased transcriptional bursting frequencies and elevated *E2A* and *E2-2* mRNA half-lives. The increase in *E2A* and *E2-2* bursting frequencies often occurred at shared interchromosomal transcriptional hubs. We suggest that in naïve B cells low *E2A* and *E2-2* bursting frequencies and high *E2A* and *E2-2* mRNA decay rates instruct noisy gene expression that allows a clonal and swift response to invading pathogens whereas in activated B cells increased transcriptional bursting and low mRNA decay rates dictate an activated B lineage gene program.

INTRODUCTION

Upon foreign antigen encounter, mature B cells undergo rapid cellular expansion and differentiation. The proliferation and differentiation of B cells occur in distinct anatomical structures, named germinal centers. In germinal centers, activated B cells undergo clonal expansion, immunoglobulin class switching recombination (CSR), and somatic hypermutation to differentiate into either plasma or memory B cells (*1*). Upon exposure to pathogens, innate and adaptive immune receptors activate the phosphatidylinositol 3-kinase (PI3K), nuclear factor κB (NF-κB), and Janus kinase–signal transducer and activator of transcription (JAK-STAT) pathways to instruct plasma cell as well as memory B cell gene programs (*2*–*5*). Prominent among the induced target genes is the activation-induced cytidine deaminase (AID) gene (*6*). AID is a deaminase that converts deoxycytidine into deoxyuridine at single-stranded DNA (*5*, *7*). Deamination of both single strands across the switch regions leads to double-stranded DNA breaks that join to promote CSR (*7*).

The activation of CSR is orchestrated by distinct stimuli that can be segregated into T cell–dependent and T cell–independent pathways (*8*, *9*). Primary signals involve either engagement of CD40 expressed on B cells with CD40 ligand that is expressed on T follicular helper (T_{FH}) cells or coordinate activation by Toll-like receptors (TLRs) and the B cell receptor (BCR) (*10*, *11*). Lipopolysaccharide (LPS) is the sole microbial agent that has the ability to directly orchestrate CSR by cross-linking TLR4 and the BCR (*9*). Naïve B cells that have engaged with antigenic stimuli swiftly respond to secondary stimuli, including interleukin-4 (IL-4), interferon γ (IFNγ), or transforming growth factor β (TGFβ), to promote CSR (*9*).

Numerous transcription factors have been identified that regulate AID expression and promote plasma cell differentiation (*12*). Prominent among transcription factors that regulate AID expression are E2A and E2-2 (*13*–*17*). The E2A and E2-2 proteins, often referred to as E-proteins, bind DNA as homodimers or heterodimers (*18*, *19*). The DNA binding activities of E-proteins are regulated by Id proteins (*20*, *21*). Four Id proteins, named Id1 to Id4, have been identified (*19*). The Id proteins contain an HLH (helix-loop-helix) domain but lack a basic region and interfere with E-protein DNA binding activity upon dimerization (*18*). In B cell progenitors, E-proteins induce a B lineage–specific gene program, activate Igh, Igκ, and Igλ rearrangement, and orchestrate receptor editing (*22*–*26*). Upon assembly of an inert BCR, E-protein abundance declines, whereas Id3 levels increase to promote developmental progression (*27*). In activated germinal center B cells, E2A proteins are again elevated to induce CSR and plasma cell differentiation (*13*–*16*).

Transcription either is continuous or occurs in bursts. In continuous transcription, polymerase recruitment is initiated at a constant rate. Continuous transcription is associated with low heterogeneity in mRNA abundance (*28*–*30*). Bursting signatures can be defined in terms of burst size, the time intervals that separate transcriptional bursts, and the extent of bursting (*31*). Transcription in bursts leads to substantial variability in mRNA abundance (*32*). Insights into mechanisms that instruct transcriptional bursting signatures remain rudimentary at best. They are plausibly instructed by chromatin folding, nuclear positioning, enhancer activity, or the repositioning of chromatin to and from transcription factories (*33*).

To determine whether and how during the course of B cell activation *E2A* and *E2-2* transcriptional bursting signatures are regulated, we measured *E2A* and *E2-2* mRNA abundance in single cells. We found that B cell activation was closely associated with an increase in *E2A* and *E2-2* mRNA abundance across the population. Close inspection of transcriptional parameters revealed that naïve B cell progenitors displayed low *E2A* and *E2-2* bursting frequencies and high mRNA degradation rates, while at later stages of activation *E2A* and *E2-2* bursting frequencies and mRNA half-lives coordinately increased. On the basis of these observations, we propose that in naïve B cells low *E2A* and *E2-2* bursting frequencies and high mRNA decay rates allow a swift clonal response to antigen exposure in a subset of cells primed to become activated, while in activated B cells high bursting frequencies and low mRNA decay rates narrow heterogeneity in mRNA abundance to activate CSR and/or instruct a plasma-specific gene program.

RESULTS

B cell activation is closely associated with an increase in *E2A* and *E2-2* mRNA abundance

In previous studies, we showed that during the course of B cell activation E2A protein levels increase (*13*). To determine whether likewise

Division of Biological Sciences, Section of Molecular Biology, University of California, San Diego, La Jolla, CA 92039, USA.
*Corresponding author. Email: cmurre@ucsd.edu

E2A transcript levels are elevated, B cells were derived from the spleen of C57Bl/6 mice, activated with LPS, and analyzed using single-molecule RNA-FISH (fluorescence in situ hybridization) using conjugated fluorescently labeled *E2A* probes. To quantify expression levels, the number of mRNA species was counted and plotted as probability distribution functions (Fig. 1). We found that *E2A* mRNA abundance was low in naïve B cells (Fig. 1A). When cultured in the presence of LPS for 2 to 4 hours, a small fraction of B cells exhibited increased *E2A* mRNA abundance (Fig. 1, B and C). *E2A* mRNA abundance substantially increased when B cells were cultured in LPS for 24 hours (Fig. 1D). *E2A* mRNA levels increased further at 48 hours but dropped 72 hours after activation (Fig. 1, E and F).

Because previous studies showed that E2A and E2-2 act in concert to promote B cell activation and AID expression, we examined *E2-2* mRNA abundance in naïve and activated B cells (*13*–*17*). Again, we used RNA-FISH coupled with conjugated fluorescently labeled

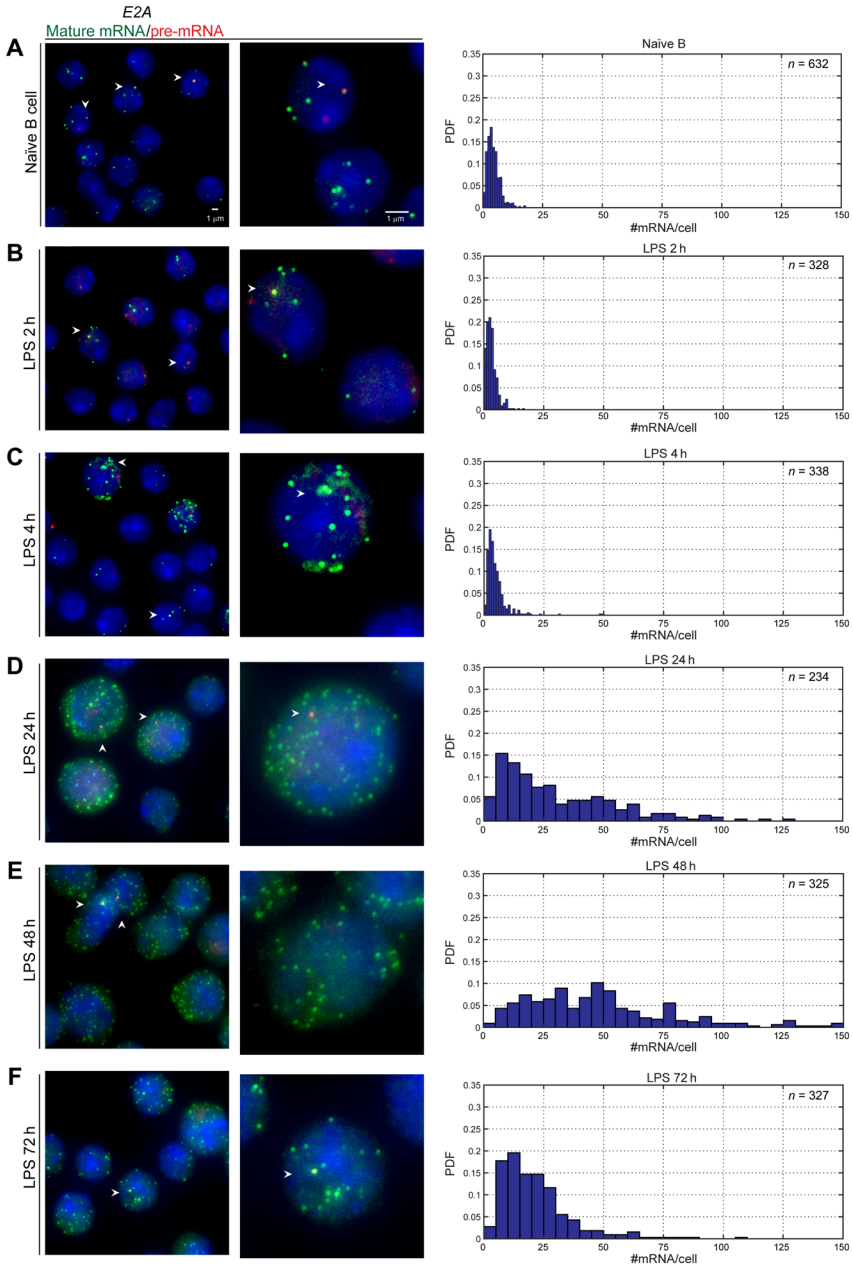

Fig. 1. *E2A* mRNA abundance is elevated during the course of B cell activation. (**A** to **F**) *E2A* transcript abundance during the course of B cell activation detected by RNA-FISH that allows single-molecule detection. Representative images are shown. Time points following stimulation with LPS are indicated. Magnified images representing single cells are shown in the middle panel. *E2A* mRNA transcripts were labeled using a library of probes corresponding to *E2A* exonic regions (green dots). Nascent transcripts were labeled using a library of probes corresponding to *E2A* intronic regions (red dots). Nuclei were stained using DAPI (blue). Scale bar, 1 μm. Arrowheads indicate *E2A* bursting sites. The right panel indicates probability distribution functions (PDF) for the number of *E2A* transcripts per cell. Numbers of cells (*n*) that are analyzed for each treatment are indicated in the histograms.

E2-2 probes. We found that in naïve B cells, *E2-2* mRNA abundance was virtually absent (Fig. 2A). B cells that were activated for a duration of 2 to 4 hours showed a modest increase in *E2-2* mRNA abundance (Fig. 2, B and C). *E2-2* mRNA levels continued to increase, reaching maximum levels 48 hours after activation before declining (Fig. 2, E and F). Collectively, these data indicate that B cell activation is closely associated with increased *E2A* and *E2-2* mRNA abundance.

During the course of B cell activation, the *E2A* and *E2-2* loci reposition from the nuclear lamina to the nuclear interior

In previous studies, we demonstrated that the *Ebf1*, *Prdm1*, and *Atf4* loci repositioned during B cell activation (*34*, *35*). To determine whether likewise changes in *E2A* and *E2-2* expression levels in activated B cells were regulated by nuclear repositioning, we performed three-dimensional FISH. To this end, naïve and LPS-activated B cells were isolated from the spleen, fixed with formaldehyde, and

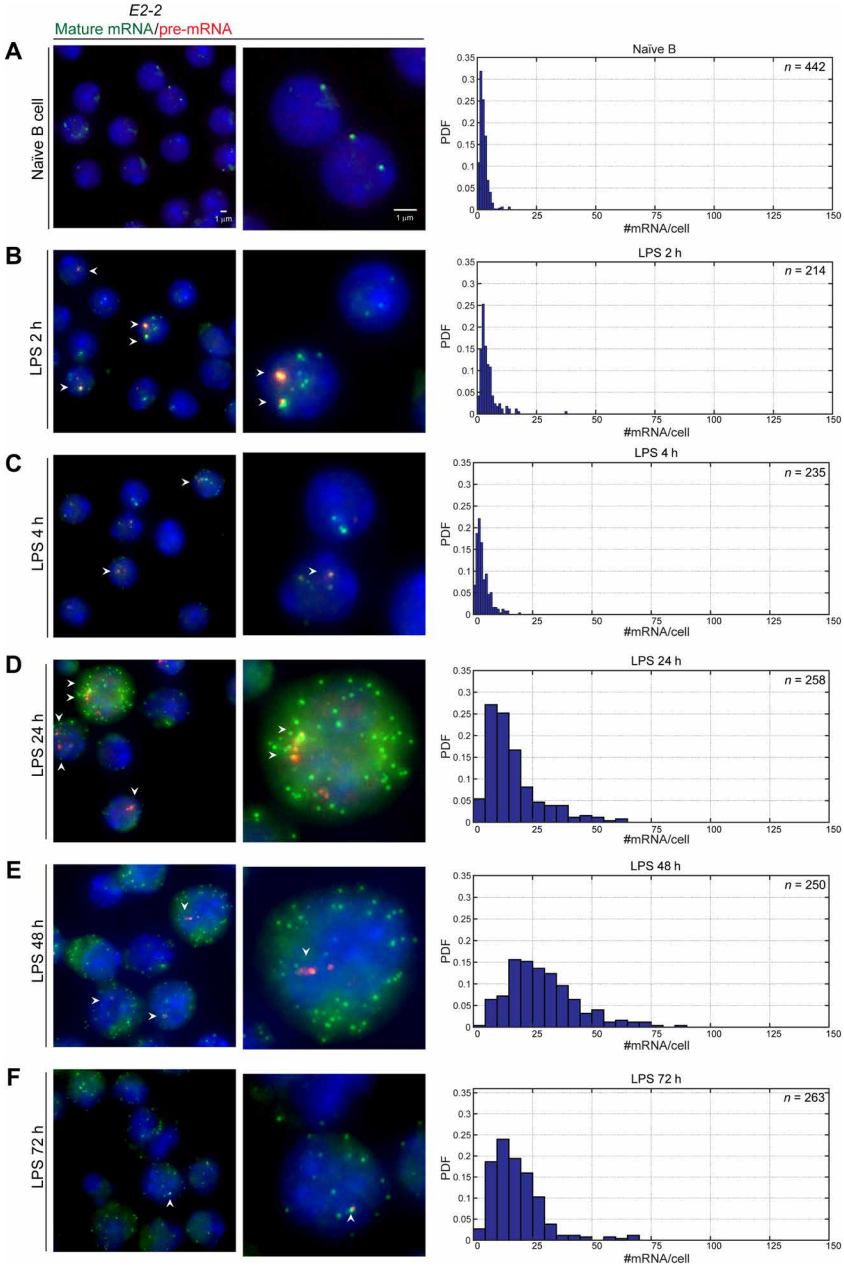

Fig. 2. *E2-2* mRNA abundance is elevated during the course of B cell activation. (**A** to **F**) *E2-2* transcript abundance during the course of B cell activation detected by RNA-FISH. Representative images are shown. Time points following stimulation with LPS are indicated. Magnified images representing single cells are shown in the middle panel. *E2-2* mRNA transcripts were labeled using a library of probes corresponding to *E2-2* exonic regions (green). Nascent transcripts were labeled using a library of probes corresponding to *E2-2* intronic regions (red). Nuclei were stained using DAPI (blue). Scale bar, 1 μm. Arrowheads indicate *E2-2* bursting sites. The right panel indicates probability distribution functions (PDF) for the number of *E2-2* transcripts per cell. Numbers of cells (*n*) that are analyzed for each treatment are indicated in the histograms.

hybridized with fluorescently labeled *E2A* and *E2-2* bacterial artificial chromosome (BAC) probes. We found that most of the naïve B cells showed at least single *E2A* and *E2-2* alleles being positioned at the nuclear lamina (fig. S1, A and B). *E2-2* alleles were more frequently associated with the nuclear lamina as compared to *E2A* alleles (fig. S1B). Upon LPS-driven activation, a significant proportion of *E2A* and *E2-2* alleles repositioned away from the lamina into the nuclear interior (fig. S1B). Thus, the increase in *E2A* and *E2-2* mRNA abundance during B cell activation is associated with nuclear repositioning of the corresponding loci away from the lamina to the nuclear interior.

E2A transcriptional bursting frequencies and mRNA decay rates fluctuate during the course of B cell activation

To identify the mechanism that underpins the changes in *E2A* mRNA abundance, we computed *E2A* bursting fractions, transcription rates, and mRNA decay rates. We used intronic probes to derive *E2A* and *E2-2* bursting frequencies (*36*). The number of *E2A* mRNAs at transcription start sites was computed from the ratio of fluorescence intensities at *E2A* and *E2-2* intronic pre-mRNAs versus exonic *E2A* and *E2-2* cytoplasmic mature mRNAs (*36*). A correction for the physical spread of the fluorescent probes that span the *E2A* locus was included in the analysis (*36*). An estimate of transcription rates at active promoters was calculated by determining polymerase II occupancy (M) at *E2A* transcription start sites from the number of nascent transcripts (*36*). The average E2A transcription rate was computed using $\mu = M\,v/L$ (v = 34 base pairs/s and L is the genomic distance spanning the *E2A* locus). mRNA decay rates (δ) were computed as the ratio of summed transcription rates measured at transcription start sites versus the number of *E2A* mRNA species.

We found that the fraction of *E2A* bursting alleles was low in naïve B cells but increased significantly 24 hours after stimulation and remained high during the course of activation (Fig. 3A). To determine whether bursting frequencies changed during the course of B cell proliferation, we labeled activated B cells with CellTrace Violet. We then sorted B cells based on CellTrace Violet staining to monitor distinct generations of dividing B cells. Sorted cells were analyzed using intronic probes spanning the *E2A* locus by RNA-FISH (fig. S2A). We found that *E2A* bursting frequencies remained equivalent for two cell divisions but increased substantially after four cell divisions, followed by a decline after five and six divisions (fig. S2B).

In contrast to the substantial changes in bursting frequencies, E2A transcription rates only modestly changed during the course of B cell activation (Fig. 3B). Akin to the changes in bursting frequencies associated with B cell activation, *E2A* mRNA half-lives also differed greatly between naïve and activated B cells (Fig. 3C). We found that in naïve B cells, *E2A* mRNA half-lives were in the order of 2 hours, while in activated B cells (24 to 48 hours) *E2A* mRNA half-lives substantially increased to 6 hours (Fig. 3C). To validate these findings, we cultured naïve and activated B cells in the presence of actinomycin D for different durations and measured mRNA abundance for the indicated time points (Fig. 3D). This analysis confirmed the computational approach described above, revealing *E2A* mRNA half-lives in the order of 2 hours for naïve versus B cells versus 6 hours for activated B cells (Fig. 3D). In summary, these data indicate that *E2A* transcriptional bursting frequencies and *E2A* mRNA half-lives are dynamic and coordinately elevated during the course of B cell activation.

During the course of B cell activation, E2A mRNA abundance and cell size are tightly correlated

The data described above revealed that elevated *E2A* and *E2-2* mRNA abundance was particularly prominent in large activated B cells (Figs. 1 and 2). To examine whether during the course of B cell activation the increase in *E2A* mRNA abundance and the increase in cell size were correlated, we plotted cell size as a function of *E2A* mRNA abundance. We found that during the course of B cell activation *E2A* mRNA abundance and size were closely correlated (fig. S3A). Next, we examined whether changes in *E2A* mRNA transcription rates and cell size were correlated during the course of B cell activation. We found that *E2A* transcription rates and cell size were not significantly correlated (fig. S3B). Thus, during the course of B cell activation, the increase in *E2A* mRNA abundance, but not transcription rates, is correlated with increased cell size.

E2-2 transcriptional bursting frequencies and mRNA decay rates are dynamic during the course of B cell activation

To determine whether during B cell activation the increase in *E2-2* mRNA abundance was also associated with alterations in bursting signatures and mRNA decay rates, we computed *E2-2* burst fractions, transcription rates, and mRNA decay rates at different time points. We found that *E2-2* bursting fractions increased in activated B cells akin to that observed for *E2A*, albeit with different magnitudes and dynamics (Fig. 4A). The frequency of *E2-2* bursting initially increased at 2 hours after activation followed by a decline at 4 hours to reach maximum levels at 24 to 48 hours (Fig. 4A). *E2-2* transcription rates were only modestly affected during the course of activation and again differed in magnitude from that of *E2A* transcription rates (Fig. 4B). *E2-2* mRNA decay rates initially remained flat but declined substantially 24 to 72 hours after activation following the same trend as observed for *E2A* mRNA decay rates (Fig. 4C). In summary, during the course of B cell activation, *E2-2* bursting frequencies and mRNA decay rates are dynamic, with naïve B cells exhibiting low *E2-2* bursting frequencies and short *E2-2* mRNA half-lives versus activated B cells showing high *E2-2* bursting frequencies and long *E2-2* mRNA half-lives.

E2A and *E2-2* alleles burst in tandem at interchromosomal transcription hubs

The data described above indicate that during the course of B cell activation *E2A* and *E2-2* mRNA abundance is elevated. To explore the possibility that *E2A* and *E2-2* mRNA levels increase coordinately, we measured *E2A* and *E2-2* mRNA abundance simultaneously in single cells (Fig. 5). We found that during the course of B cell activation *E2A* and *E2-2* mRNA abundance increased coordinately (Fig. 5). Naïve B cells showed relatively low *E2A* and *E2-2* mRNA abundance, while activated B cells showed concomitant elevated *E2A* and *E2-2* mRNA levels (Fig. 5). To reveal the mechanism that underpins the coordinate increase in *E2A* and *E2-2* mRNA abundance, we used dual-labeled intronic probes (Fig. 6A). We found that a substantial fraction of activated B cells showed coordinate *E2A* and *E2-2* bursting (Fig. 6, A and B). Notably, coordinate *E2A* and *E2-2* bursting was frequently, albeit not exclusively, associated with double-labeled (yellow) fluorescent foci (Fig. 6A). To quantitatively determine whether *E2A* and *E2-2* bursting is enriched at shared transcription hubs, we measured the spatial distances separating the *E2A* and *E2-2* fluorescent foci. We found that, using fixation conditions applied in RNA-FISH, a substantial fraction of bursting *E2A* and *E2-2* alleles

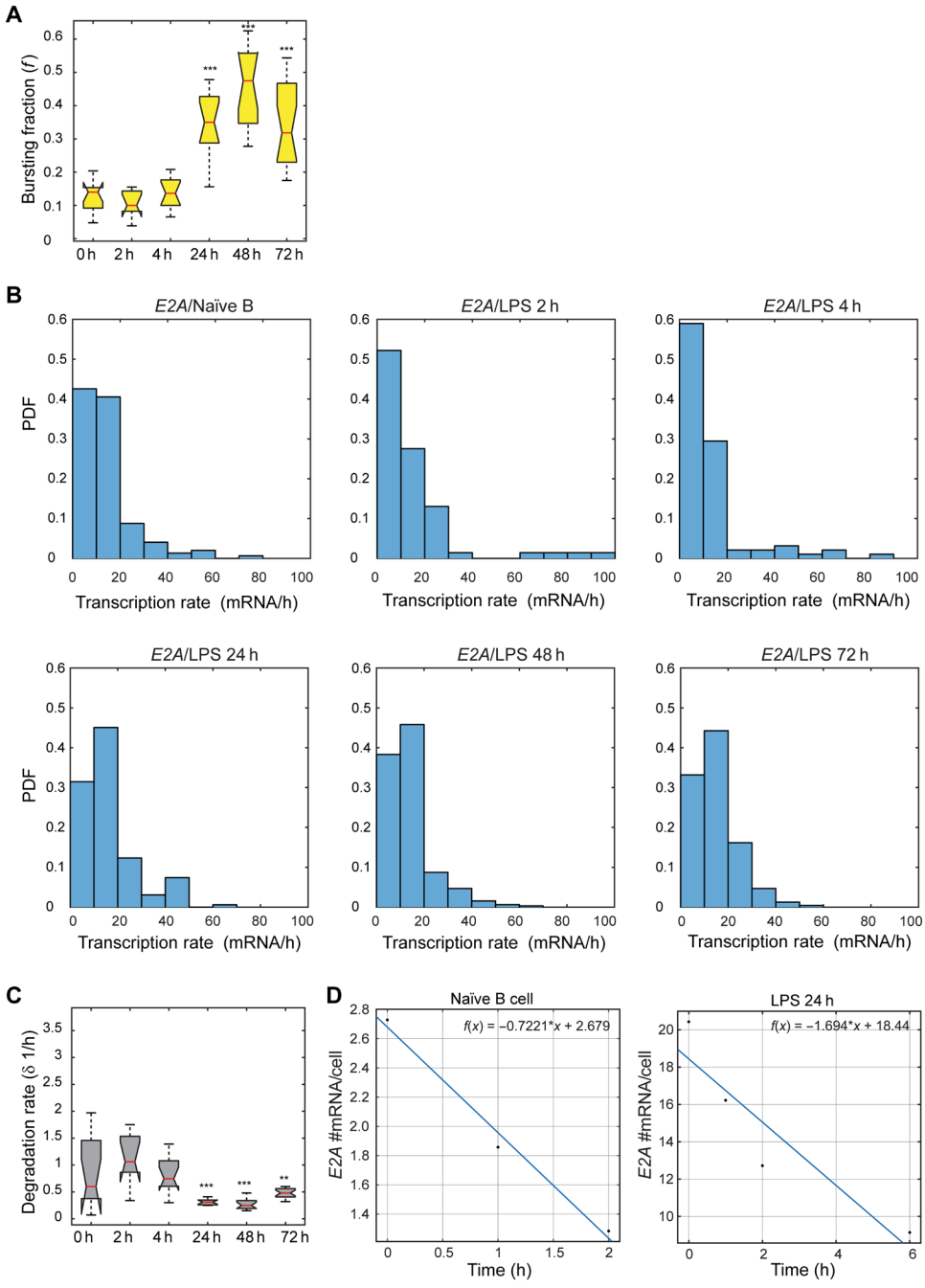

Fig. 3. *E2A* bursting frequencies and mRNA decay rates are altered during the course of B cell activation. (**A**) *E2A* bursting fractions (*f*) are indicated during the course of B cell activation. Box plots show mean and SD for *E2A* bursting fractions. *E2A* bursting fractions are shown for naïve cells and activated B cells. Time points of activation are indicated. ***$P < 0.001$. (**B**) Probability distribution functions (PDF) for *E2A* mRNA transcription rates are indicated during the course of B cell activation. Time points of activation are shown for histograms (top). (**C**) *E2A* mRNA degradation rates are shown during the course of B cell activation. Box plots show means and SDs for *E2A* bursting fractions. Time points for activation are shown. **$P < 0.01$, ***$P < 0.001$. (**D**) *E2A* mRNA decay rates as revealed by culturing naïve and activated B cells in the presence of actinomycin D. *E2A* mRNA abundance was determined using RNA-FISH. *E2A* mRNA half-lives were computed for 101 naïve B cell data for each of the indicated times ($R^2 = 0.9835$). Likewise, *E2A* mRNA half-lives were computed for activated B cells (24 hours) for the indicated time periods ($R^2 = 0.8779$). Average numbers are indicated for the indicated time points.

were located within relatively close spatial proximity from each other (Fig. 6C). Together, these data suggest that a significant fraction of *E2A* and *E2-2* alleles burst in synchrony at shared interchromosomal transcription hubs.

DISCUSSION

During the past two decades, transcriptional circuitries have been identified that, in response to antigen, promote B cell activation (*2*). Particularly prominent is a regulatory network, composed of *Irf4*,

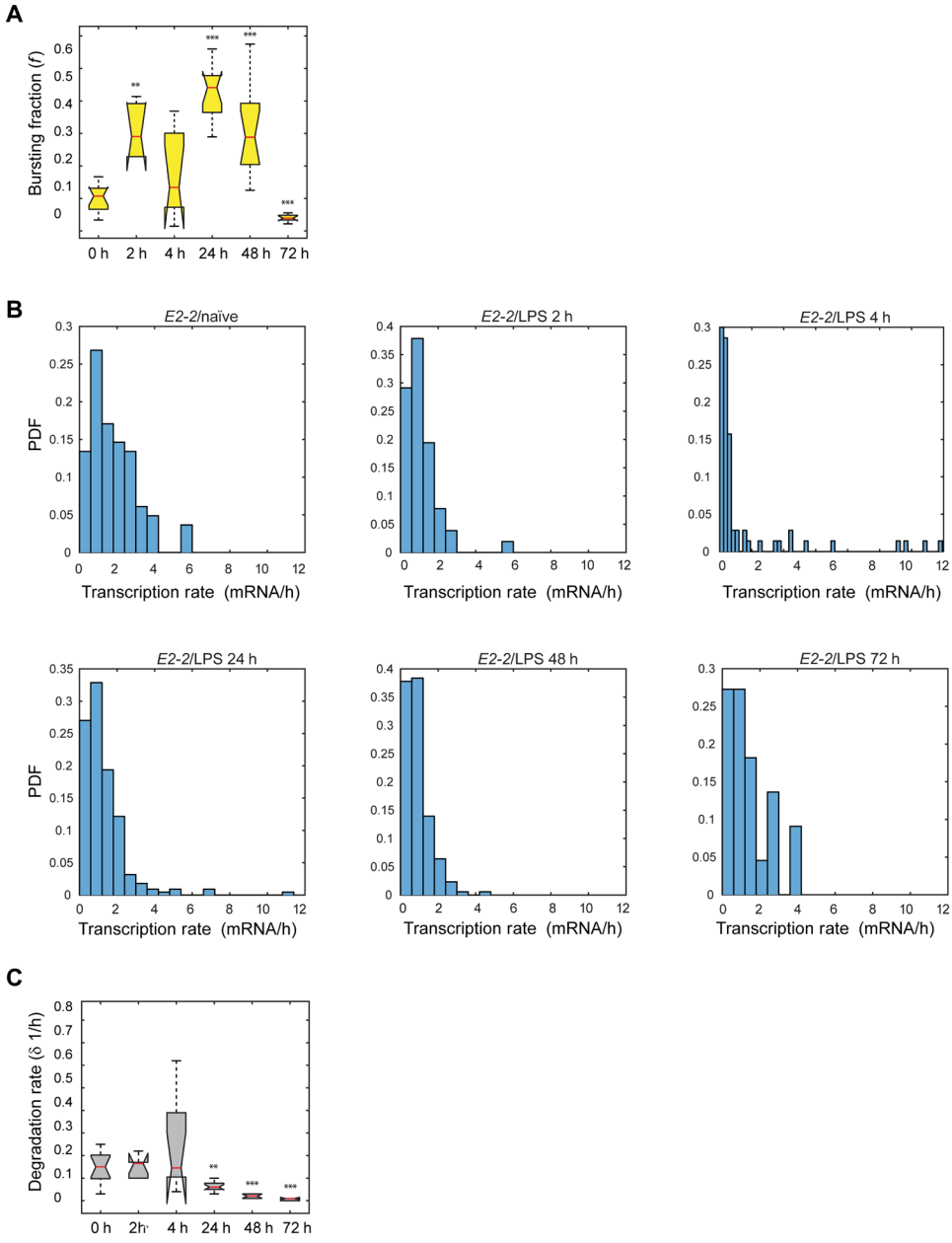

Fig. 4. *E2-2* bursting signatures and mRNA decay rates are modulated during the course of B cell activation. (**A**) *E2-2* bursting fractions are indicated during the course of B cell activation. Box plots show mean and SD for *E2-2* bursting. *E2-2* bursting fractions are shown for naïve and activated B cells. Time points of activation are indicated. ***$P < 0.001$. (**B**) Probability distribution functions (PDF) for *E2-2* mRNA transcription rates during the course of B cell activation. Time points for activation are shown for each histograms (top). (**C**) *E2-2* degradation rates are shown for the indicated time points during the course of B cell. Box plots show means and SDs for *E2-2* mRNA degradation rates. Time points of activation are shown.

Blimp, and *Bcl6*, that orchestrates the germinal center reaction (*12*). Parallel studies implicated the basic helix-loop-helix proteins, E2A and E2-2, as regulators that dictate B cell activation (*13*–*16*). While a role for these transcription factors in orchestrating B cell activation has been well documented, insights as to how they are regulated have remained rudimentary. As a first approach to address this question, we examined *E2A* and *E2-2* mRNA abundance, bursting frequencies, transcription rates, and mRNA half-lives during the course of B cell activation. We found that *E2A* and *E2-2* transcription was not continuous but rather occurred in bursts. In naïve follicular B cells, E2A bursting frequencies were low. At later stages, *E2A* bursting frequencies were swiftly elevated and frequently occurred in synergy with *E2-2* at shared interchromosomal transcription hubs. Interchromosomal hubs have been observed previously during the course of B cell activation. Specifically, the *Atf4*, *Xbp1,* and *Prdm1* loci associate at interchromosomal sites to orchestrate a plasma cell–specific gene program (*35*). It is well established that actively transcribing ribosomal RNA genes also assemble at interchromosomal transcription hubs to orchestrate ribosome genesis (*37*). In olfactory neurons, multiple enhancers assemble at interchromosomal transcription hubs

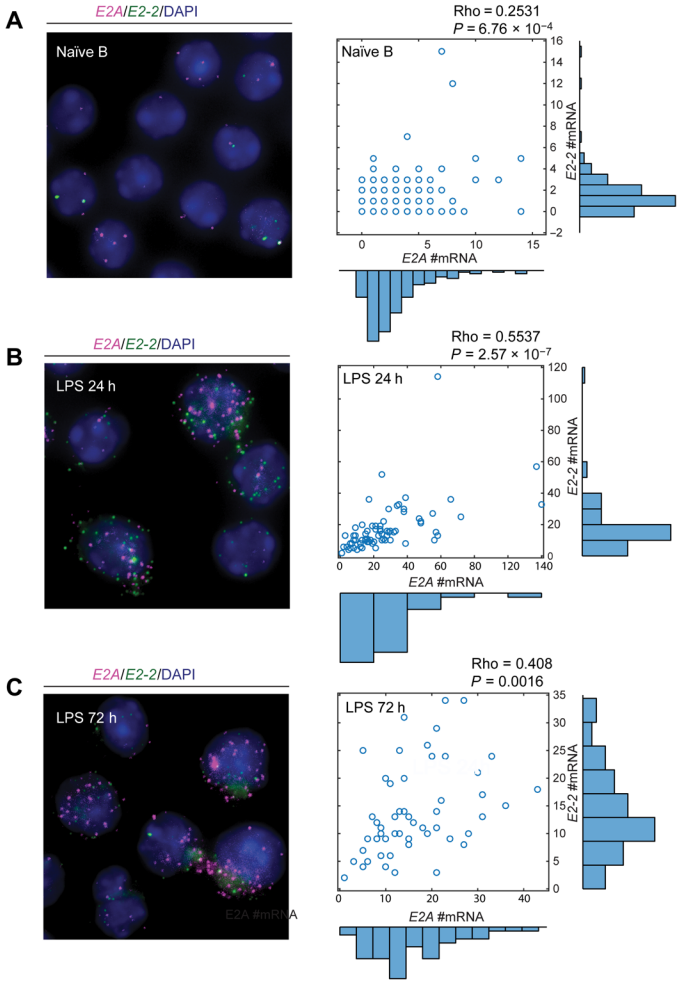

Fig. 5. Coordinate increase in *E2A* and *E2-2* mRNA abundance during the course of B cell activation. (**A** to **C**) *E2A* and *E2-2* transcript abundance in naïve B cells and activated B cells. Left panels show representative images. *E2A* (magenta) and *E2-2* transcripts (green) were labeled simultaneously in single cells using a library of probes corresponding to *E2A* and *E2-2* exonic regions. Right panels show *E2A* and *E2-2* mRNA abundance in single cells. Pearson correlation (Rho) and the likelihood (*P*) measured by chi-square test are indicated. Nuclei were visualized using DAPI staining.

to instruct olfactory receptor gene expression (*38*, *39*). Why are *E2A* and *E2-2* loci transcribed at shared interchromosomal transcription hubs rather than independently from each other? Coordinate regulation at shared interchromosomal hubs might ensure that proper ratios of E2A and E2-2 homodimers and/or heterodimers are assembled to dictate with great temporal precision lineage-specific gene programs.

In addition to orchestrating lineage-specific gene programs, the data suggest that the E-protein module also controls B cell growth. Previous studies revealed that the E-Id protein module regulates the expression of c-myc and components involved in PI3K and mammalian target of rapamycin (mTOR)–mediated signaling (*40*–*42*). These findings are consistent with a model in which E2A, c-myc, and the PI3K-mTOR module are linked to control B cell size. Thus, the E-protein module may act in parallel pathways that orchestrate B lineage–specific gene programs and metabolic pathways that instruct cell size.

E2A and *E2-2* mRNA abundance during the course of B cell activation is not only dictated by alterations in bursting frequencies. We found that the rise and fall of mRNA abundance was accompanied by large-scale changes in mRNA lifetimes. Naïve follicular B cells were associated with high *E2A* and *E2-2* mRNA decay rates, while at later stages *E2A* and *E2-2* mRNA half-lives increased. How are these alterations in mRNA decay rates during B cell activation established? We suggest that they involve microRNA (miRNA)–mediated decay pathways. It will be important to identify putative miRNAs that target *E2A* and *E2-2* mRNA abundance and determine whether and how they modulate B cell activation.

The data bring into question as to whether and how differences in *E2A* and *E2-2* bursting frequencies and mRNA life-times relate to B cell activation. In naïve B cells, relatively low bursting frequencies are coordinated with high mRNA decay rates to lower overall *E2A* and *E2-2* mRNA abundance. Upon antigen exposure, however, *E2A* and *E2-2* increased bursting frequencies and reduced mRNA decay rates readily result in high E2A and E2-2 mRNA abundance. Do these alterations in mRNA abundance relate to changes in protein levels? Early studies revealed that E47 protein abundance is low in naïve B cells but readily accumulates to relatively high levels in activated B cells (*13*). In addition, akin to *E2A* mRNA abundance, E47 protein levels are quite heterogeneous in naïve B cells (*13*). While most of the naïve B cells showed barely detectable E47 protein levels, a few cells displayed relatively high E47 protein abundance, again revealing heterogeneity of E47 expression across the population (*13*). We suggest that the noise in E47 gene expression is caused, at least in part, by low bursting frequencies and high mRNA decay rates. *E2A* and *E2-2* heterogeneity may allow a fast and clonal response in cells that are undergoing transcriptional bursting at the time that naïve B cells are exposed to antigen. In contrast, in activated B cells, increased *E2A* and *E2-2* bursting frequencies and lower mRNA decay rates may dampen *E2A* and *E2-2* gene expression noise to promote the coordinate rise in E2A and E2-2 protein abundance.

The data raise the question whether similar mechanisms dictate the immune response in other cell types. Memory versus effector cell fate might very well be instructed by changes in bursting frequencies of HLH genes, RNA decay pathways, and heterogeneity in HLH mRNA abundance during the course of antigen exposure (*43*). Likewise, do the E2A, HEB, and E2-2 loci also burst in concert in common lymphoid progenitors (CLPs)? Is there a necessity for *E2A*, *E2-2*, and *HEB* coordinate transcriptional bursting programs and modulation of mRNA decay rates to establish B and T cell identity? Does intrinsic heterogeneity in mRNAs and bursting frequencies of genes encoding for transcriptional regulators in the lymphoid-myeloid primed progenitor (LMPP) or CLP compartments underpin the mechanism that instructs innate and immune cell fate? Early pioneering studies indicated heterogeneity in mRNAs associated with transcriptional regulators across hematopoietic compartments that specify adaptive immune cell fate (*44*). On the basis of the observations described here, we suggest that HLH mRNA heterogeneity in early lymphoid progenitors is instructed by a combination of "bursty" gene expression programs and mRNA decay pathways. During the past three decades, much has been learned about factors and pathways that control immune cell development. However, insights into temporal mechanisms that orchestrate immune cell development remain rudimentary. Live cell imaging studies that monitor HLH gene expression in space and time should help to illuminate temporal mechanisms that underpin immune cell development and immune cell activation.

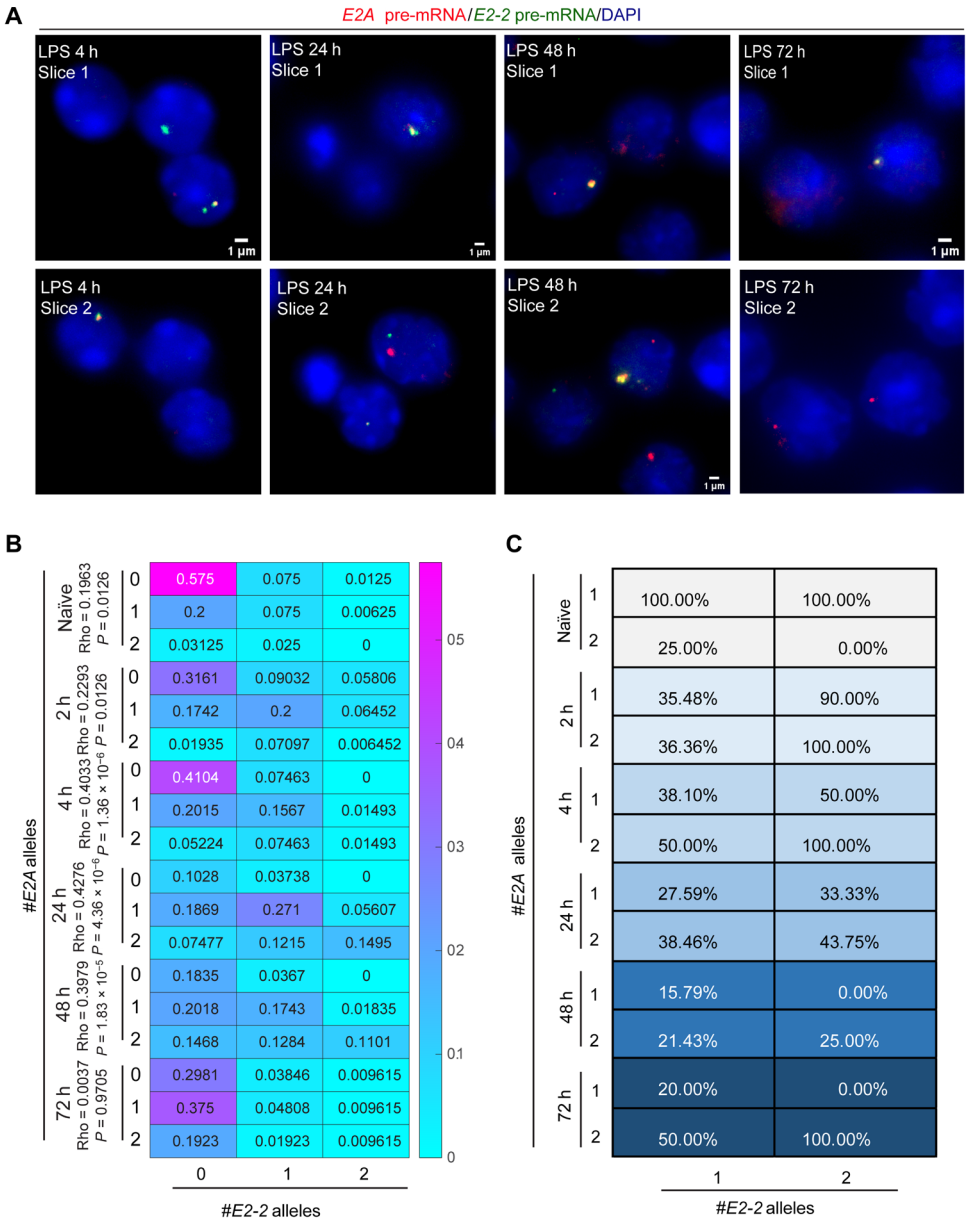

Fig. 6. *E2A* and *E2-2* alleles burst in tandem at interchromosomal transcription hubs. (**A**) Representative images indicating *E2A* and *E2-2* bursty gene expression during the course of B cell activation. The top and bottom images are sections that were derived from the same z-stack. Intronic regions were fluorescently labeled to reveal nascent transcription. Red fluorescent foci are indicative of *E2A* bursting alleles. Green fluorescent foci are indicative of *E2-2* transcriptional bursting. (**B**) Heatmap displaying the percentages of cells that show allelic *E2A* and/or *E2-2* expression in single cells during the course of B cell activation. Naïve and different time points for the duration of B cell activation are shown. Chi-square test and Pearson correlation (Rho) are indicated. (**C**) Table showing the percentage of co-bursting *E2A* and *E2-2* alleles.

MATERIALS AND METHODS

Mice and cell culture

Adult C57/B6 mice were purchased from The Jackson Laboratory and maintained in a specific pathogen–free facility at the University of California, San Diego. Mice were analyzed at 8 weeks of age. Both male and female mice were used for analysis. Animal studies (S00031) were approved by the Institutional Animal Care and Use Committee. Splenocytes were incubated with CD23-biotin (eBioscience, clone B3B4) and purified using anti-biotin microbeads (Miltenyi Biotec). Sorted B cells were cultured for up to 3 days in RPMI 1640 medium supplemented with 10% fetal bovine serum (FBS), antibiotics, 2 mM L-glutamine, and 50 μM β-mercaptoethanol at 37°C and 5% CO_2. LPS (*Escherichia coli*, Sigma-Aldrich, L2654) was used at 10 μg/ml for B cell activation.

Imaging

Library of probe sets was designed and purchased from LGC Biosearch Technology. Probe library sequences are attached (table S1). B cells were placed on poly-L-lysine–coated coverslips at 37°C for 20 min, formaldehyde-fixed, permeabilized in 70% ethanol, and stored at 4°C overnight. The coverslips were washed and incubated in buffer (10% formamide in 2× SSC) for 10 min at room temperature.

Next, coverslips were incubated with probes in hybridization buffer (10% formamide and 10% dextran in 2× SSC) at 37°C overnight in a humidified hybridization oven. The following morning, coverslips were rinsed in washing solution and washed twice for 30 min each at 37°C. DAPI (4′,6-diamidino-2-phenylindole) was added at the second wash to mark the nuclei. Coverslips were rinsed once in 2× SSC at room temperature and mounted with Prolong Gold Anti-Fade reagents. Slides were dried in the dark overnight before imaging. Three-dimensional images were acquired using Applied Precision Inverted Deconvolution Deltavision Microscope with a 100× objective (Nikon 100×). Optical sections (z-stacks) separated by 0.2 μm were obtained across the cell volume in DAPI, fluorescein isothiocyanate (FITC), Texas Red, and Cy5 channels. For naïve B cells and B cells stimulated with LPS for 2 or 4 hours, cell volumes were taken for stacks of 20 optical sections. For B cells stimulated in the presence of LPS for 24, 48, and 72 hours, cell volumes were analyzed using 25 z-stacks. Bursting fractions (*f*) were determined by computing the fraction of E2A and E2-2 exonic and intronic fluorescent foci across the population (*38*). Images were analyzed by Trans-Quant software in MATLAB. mRNA numbers were counted, and transcription and mRNA decay rates were calculated using Trans-Quant.

Three-dimensional DNA-FISH

Probe library constructions, lamina staining, hybridization procedures, and imaging conditions were previously described (*35*). BAC probes corresponding to the E2A (RP24-339 K23) and for E2-2 (RP24-125G3) loci were obtained from the BACPAC Resource Center (BPRC) at the Children's Hospital Oakland Research Institute.

Actinomycin D treatment

For testing naïve B cell degradation, sorted naïve B cells were suspended in B cell medium [RPMI 1640 medium supplemented with 10% FBS, antibiotics, 2 mM L-glutamine, 50 mM β-mercaptoethanol, and LPS (10 mg/ml)] at 37°C and 5% CO_2. Actinomycin D (Sigma-Aldrich, A9415-2MG) was suspended in the medium at the final concentration of 10 μg/ml. Cells were seeded in 24-well plates and were later harvested at 0.5, 1, 1.5, and 2 hours and analyzed using RNA-FISH. For testing degradation of activated B cells, sorted naïve B cells were seeded in B cell medium; after 24 hours, actinomycin D (10 mg/ml) was added into the B cell medium and cells were harvested at 2, 4, and 6 hours for either RNA-FISH or quantitative polymerase chain reaction (qPCR). qPCR primers were as follows: E2A, 5′-AGTCTCAGAGAATGGCACCCGTG (forward) and 5′-ACCTTCGCTGTATGTCCGGCTAG (reverse); E2-2, 5′-CCAACAGCGAATGGCTGCCTTAG (forward) and 5′-TGACCCAAGATCCCTGCTAGTCATG (reverse).

CellTrace Violet cell labeling and sorting

Naïve B cells were labeled with 7 μM CellTrace Violet dye (Thermo Fisher Scientific, C34571). Cells were cultured for 3 days in RPMI 1640 medium supplemented with 10% FBS, antibiotics, 2 mM L-glutamine, and 50 μM β-mercaptoethanol and activated with LPS (10 μg/ml) at 37°C and 5% CO_2. Identification of each cell division was based using the CellTrace Violet Cell Proliferation Kit. Cell division cycles were sorted using a three-laser FACSAria Fusion.

SUPPLEMENTARY MATERIALS

Supplementary material for this article is available at https://science.org/doi/10.1126/sciadv.abm0819

REFERENCES AND NOTES

1. C. C. Goodnow, K. L. Vinuesa, F. Randall, R. Mackay, Control systems and decision making for antibody production. *Nat. Immunol.* **11**, 681–688 (2010).
2. V. Chandra, A. Bortnick, C. Murre, AID targeting: Old mysteries and new challenges. *Trends Immunol.* **36**, 527–535 (2015).
3. G. Teng, F. N. Papavasiliou, Immunoglobulin somatic hypermutation. *Annu. Rev. Genet.* **41**, 107–120 (2007).
4. M. McHeyzer-Williams, S. Okitsu, N. Wang, L. McHeyzer-Williams, Molecular programming of B cell memory. *Nat. Rev. Immunol.* **12**, 24–34 (2012).
5. L. Kato, A. Stanlie, N. A. Begum, M. Kobayashi, M. Aida, T. Honjo, An evolutionary view of the mechanism for immune and genome diversity. *J. Immunol.* **188**, 3559–3566 (2012).
6. M. Muramatsu, K. Kinoshita, S. Fagarasan, S. Yamada, Y. Shinkai, T. Honjo, Class switch recombination and hypermutation require activation-induced cytidine deaminase (AID), a potential RNA editing enzyme. *Cell* **102**, 553–563 (2000).
7. Z. Xu, H. Zan, E. J. Pon, T. Mai, P. Casali, Immunoglobulin class-switch DNA recombination: Induction, targeting and beyond. *Nat. Rev. Immunol.* **12**, 517–531 (2012).
8. A. Cerutti, I. Puga, M. Cols, Innate control of B cell responses. *Trends Immunol.* **32**, 202–211 (2011).
9. E. J. Pone, J. Zhang, T. Mai, C. A. White, G. Li, J. Sakakura, P. J. Patel, A. Al-Qahtani, H. Zan, Z. Xu, P. Casali, BCR-signalling synergizes with TLR-signalling for induction of AID and immunoglobulin class-switching through the non-canonical NF-κB pathway. *Nat. Commun.* **3**, 767–774 (2012).
10. G. A. Bishop, B. S. Hostager, The CD40-CD154 interaction in B cell-T cell liaisons. *Cytokine Growth Factor Rev.* **14**, 297–309 (2003).
11. G. A. Bishop, The many faces of CD40: Multiple roles in normal immunity and disease. *Semin. Immunol.* **21**, 255–256 (2009).
12. S. L. Nutt, N. Taubenheim, J. Hasbold, L. M. Corcoran, P. D. Hodgkin, The genetic network controlling plasma cell differentiation. *Semin. Immunol.* **23**, 341–349 (2011).
13. M. W. Quong, D. P. Harris, S. L. Swain, C. Murre, E2A activity is induced during B cell activation to promote immunoglobulin class switch recombination. *EMBO J.* **18**, 6307–6318 (1999).
14. C. E. Sayegh, M. W. Quong, Y. Agata, C. Murre, E-proteins directly regulate expression of activation-induced deaminase in mature B cells. *Nat. Immunol.* **4**, 586–593 (2003).
15. M. Wöhner, H. Tagoh, I. Bilic, M. Jaritz, D. K. Poliakova, M. Fischer, M. Busslinger, Molecular functions of the transcription factors E2A and E2-2 in controlling germinal B cell and plasma cell development. *J. Exp. Med.* **213**, 1201–1221 (2016).
16. R. Gloury, D. Zotos, M. Zuidscherwoude, F. Masson, Y. Liao, J. Hasbold, L. M. Corcoran, P. D. Hodgkin, G. T. Belz, W. Shi, S. L. Nutt, D. M. Tarlinton, A. Kallies, Dynamic changes in Id3 and E-protein activity orchestrate germinal center and plasma cell development. *J. Exp. Med.* **213**, 1095–1111 (2016).
17. S. Chen, M. Miyazaki, V. Chandra, K. M. Fisch, A. N. Chang, C. Murre, Id3 orchestrates germinal center B cell development. *Mol. Cell. Biol.* **36**, 2543–2552 (2016).
18. G. Bain, C. Murre, The role of E-proteins in B- and T-lymphocyte development. *Semin. Immunol.* **10**, 143–153 (1998).
19. C. Murre, Helix-loop-helix proteins and the advent of cellular diversity: 30 years of discovery. *Genes Dev.* **33**, 6–25 (2019).
20. R. Benezra, R. L. Davis, D. Lockshon, D. L. Turner, H. Weintaub, The protein Id: A negative regulator of helix-loop-helix DNA binding proteins. *Cell* **61**, 49–59 (1990).
21. Y. Yokota, A. Mansouri, S. Mori, S. Sugawara, S. Adachi, S. Nishikawa, P. Gruss, Development of peripheral lymphoid organs and natural killer cells depends on the helix-loop-helix protein Id2. *Nature* **397**, 702–706 (1999).
22. G. Bain, E. C. Maandag, D. J. Izon, D. Amsen, A. M. Kruisbeek, B. C. Weintraub, I. Krop, M. S. Schlissel, A. Feeney, M. van Roon, A. Berns, C. Murre, E2A proteins are required for proper B cell development and initiation of immunoglobulin gene rearrangements. *Cell* **79**, 885–892 (1994).
23. Y. Zhuang, P. Soriano, H. Weintraub, The helix-loop-helix gene E2A is required for B cell formation. *Cell* **79**, 875–884 (1994).
24. K. Beck, M. M. Peak, T. Ota, D. Nemazee, C. Murre, Distinct roles for E12 and E47 in B cell specification and the sequential rearrangement of immunoglobulin light chain loci. *J. Exp. Med.* **206**, 2271–2284 (2009).
25. K. Kwon, C. Hutter, Q. Sun, I. Bilic, C. Cobaleda, S. Malin, M. Busslinger, Instructive role of the transcription factor E2A in early B lymphopoiesis and germinal center B cell development. *Immunity* **28**, 751–762 (2008).
26. M. Miyazaki, K. Miyazaki, K. Chen, Y. Jin, J. Turner, A. J. Moore, R. Saito, K. Yoshida, S. Ogawa, H.-R. Rodewald, Y. C. Lin, H. Kawamoto, C. Murre, The E-Id protein axis specifies adaptive lymphoid cell identity and suppresses thymic innate lymphoid cell development. *Immunity* **46**, 818–834.e4 (2017).
27. M. Quong, A. Martensson, A. W. Langerak, R. R. Rivera, D. Nemazee, C. Murre, Receptor editing and marginal zone B cell development are regulated by the helix-loop-helix protein, E2A. *J. Exp. Med.* **199**, 1113–1120 (2004).

28. W. J. Blake, M. Kaern, C. R. Cantor, J. J. Collins, Noise in eukaryotic gene expression. *Nature* **422**, 633–637 (2003).
29. J. M. Raser, E. K. O'Shea, Control of stochasticity in eukaryotic gene expression. *Science* **304**, 1811–1814 (2004).
30. A. Raj, A. van Oudenaarden, Nature, nurture, or chance: Stochastic gene expression and its consequences. *Cell* **135**, 216–226 (2008).
31. I. Golding, J. Paulsson, S. M. Zawilski, E. C. Cox, Real-time kinetics of gene activity in individual bacteria. *Cell* **123**, 1025–1036 (2005).
32. A. Eldar, M. B. Elowitz, Functional roles for noise in genetic circuits. *Nature* **467**, 167–173 (2010).
33. T. Fukaya, B. Lim, M. Levine, Enhancer control of transcriptional bursting. *Cell* **166**, 358–368 (2016).
34. Y. C. Lin, C. Benner, R. Mansson, S. Heinz, K. Miyazaki, M. Miyazaki, V. Chandra, C. Bossen, C. K. Glass, C. Murre, Global changes in nuclear positioning of genes and intra- and interdomain genomic interactions that orchestrate B cell fate. *Nat. Immunol.* **12**, 1196–1204 (2012).
35. A. Bortnick, Z. He, M. Aubrey, V. Chandra, M. Denholtz, K. Chen, Y. C. Lin, C. Murre, Plasma cell fate is orchestrated by elaborate changes in genome compartmentalization and inter-chromosomal hubs. *Cell Rep.* **31**, 107876 (2020).
36. K. Halpern, S. Tanami, S. Landen, M. Chapal, L. Szlak, A. Hutzler, A. Nizhberg, S. Itzkovitz, Bursty gene expression in the intact mammalian liver. *Mol. Cell* **58**, 147–156 (2015).
37. B. McStay, Nucleolar organizer regions: Genomic 'dark matter' requiring illumination. *Genes Dev.* **30**, 1598–1610 (2016).
38. S. Lomvardas, G. Barnea, D. J. Pisapia, M. Medelsohn, J. Kirkland, R. Axel, Interchromosomal interactions and olfactory receptor choice. *Cell* **126**, 403–413 (2006).
39. K. Monahan, S. Lomvardas, Monoallelic expression of olfactory receptors. *Annu. Rev. Cell Dev. Biol.* **31**, 721–740 (2015).
40. M. Miyazaki, K. Miyazaki, S. Chen, V. Chandra, K. Wagatsuma, Y. Agata, H.-R. Rodewald, R. Saito, A. N. Chang, N. Varki, H. Kawamoto, C. Murre, The E-Id protein axis modulates the activities of the PI3K-AKT-mTORC1-Hif1a and c-myc/P19Arf pathways to suppress innate variant TFH cell development, thymocyte expansion, and lymphomagenesis. *Genes Dev.* **29**, 409–425 (2015).
41. D. P. Calado, Y. Sasaki, S. A. Godinho, A. Pellerin, K. Köchert, B. P. Sleckman, I. M. de Alborán, M. Janz, S. Rodig, K. Rajewsky, The cell-cycle regulator c-myc is essential for the formation and maintenance of germinal centers. *Nat. Immunol.* **13**, 1092–1100 (2012).
42. J. Jellusova, R. C. Rickert, The PI3K pathway in B cell metabolism. *Crit. Rev. Biochem. Mol. Biol.* **51**, 359–378 (2016).
43. K. D. Omilusik, L. A. Shaw, A. W. Goldrath, Remembering one's ID/E-ntity: E/ID protein regulation of T cell memory. *Curr. Opin. Immunol.* **5**, 660–666 (2013).
44. R. Mansson, R. Zandi, E. Welinder, P. Tsapogas, N. Sakaguchi, D. Bryder, M. Sigvardsson, Single-cell analysis of the common lymphoid progenitor compartment reveals functional and molecular heterogeneity. *Blood* **115**, 2601–2609 (2010).

Acknowledgments: We thank members of the Murre laboratory for comments and suggestions. Imaging was performed at the University of California, San Diego School of Medicine Microscopy Core (P30 NS047101). **Funding:** Y.Z. and C.M. were supported by the NIH (R01 AI082850, RO1 AI102853, and RO1 AI100880). **Author contributions:** Y.Z. and C.M. designed experiments. Y.Z. and C.M. wrote the manuscript. **Competing interests:** The authors declare that they have no competing interests. **Data and materials availability:** All data needed to evaluate the conclusions in the paper are present in the paper and/or the Supplementary Materials.

Submitted 25 August 2021
Accepted 14 October 2021
Published 3 December 2021
10.1126/sciadv.abm0819